Clays and Clay Minerals, Vol. 42, No. 3, 308–320, 1994.

FTIR REFLECTANCE *vs.* EPR STUDIES OF STRUCTURAL IRON IN KAOLINITES

THIERRY DELINEAU,[1] THIERRY ALLARD,[2] JEAN-PIERRE MULLER,[2,3] ODILE BARRES,[1] JACQUES YVON,[1] AND JEAN-MAURICE CASES[1]

[1] Laboratoire Environnement et Minéralurige, UA 235 CNRS, ENSG-INPL, B.P.40, 54501 Vandoeuvre Cédex, France

[2] Laboratoire de Minéralogie et Cristallographie, Universités Paris VI et VII, 4, Place Jussieu, 75252 Paris Cedex 05, France

[3] O.R.S.T.O.M., Départment T.O.A., UR1G, 213, rue Lafayette, 75480 Paris Cedex 10, France

Abstract—The substitution of Fe^{3+} in the kaolinite structure is studied by EPR spectrometry and by FTIR spectrometry on a large set of kaolins from different origins (sedimentary and primary ores, soil kaolins). The IR bands at 3598 and 875 cm^{-1}, observed in the literature only in the case of disordered kaolins or in Fe-rich environments (synthetic, lateritic), are revealed by high-resolution IR analysis, whatever the origin and the total Fe content of the samples. The EPR bands corresponding to Fe^{3+} substituted in sites II of the octahedral sheet increase when the IR absorbance near 3600 cm^{-1} increases. Two IR absorption bands near 4465 cm^{-1} and 7025 cm^{-1} are observed for the first time, both in transmission and diffuse reflectance on all samples. These bands are assigned to the combination of the 3598 and 875 cm^{-1} bands and to the first harmonic of the band at 3598 cm^{-1}, respectively. The area of the band at 4465 cm^{-1} in diffuse reflectance is quantitatively correlated to the abundance of Fe^{3+} located in centers II as measured by ESR. This directly confirms the assignment of the two IR bands at 3598 and 875 cm^{-1} to OH stretching and deformation vibration bands in octahedral FE^{3+} environment in the kaolinite structure, respectively. Effects due to the size of particles and to the main kaolins impurities on the near infrared spectra, are also discussed.

Key Words—EPR, Fe, Kaolinite, Mid and near infrared, Substitution.

INTRODUCTION

Kaolinite, an ubiquitous clay mineral at the Earth's surface (Murray, 1988), is known to incorporate defects of various types, either extended (e.g., stacking faults) or localized (e.g., impurities), which are related to the condition of genesis of this mineral (Cases *et al.*, 1982; Giese, 1988). Among the latter, structural trivalent Fe is of special importance as it occurs as the main impurity in all natural kaolinites (Muller and Calas, 1993) and influences several macroscopic properties, such as the degree of disorder and the particle size (Meads and Malden, 1975; Herbillon *et al.*, 1976; Mestdagh *et al.*, 1980; Cases *et al.*, 1982; Muller and Bocquier, 1987).

On account of its high sensitivity, electron paramagnetic resonance (EPR) is probably the most convenient technique for studying both the distribution and content of structural Fe in kaolinite (cf. reviews by Hall, 1980; Pinnavaia, 1981; Muller and Calas 1993). Infrared spectroscopy has also been used for the same purpose. Nevertheless, some uncertainties remain concerning the assignment of IR absorption features to the presence of trivalent Fe in kaolinite structure. According to Mendelovici *et al.* (1979), Fe in the octahedral sheet of lateritic kaolinites is characterized by two absorption bands, at 865–875 and 3607 cm^{-1}, assigned as δ Al–OH–Fe and νOH, respectively. However, the detection of the 865cm^{-1} band required a special preparation: CsCl was used for pelletization. The pellets were further heated to 270°C in order to delaminate the clay through the formation of a kaolinite–CsCl–H_2O complex. The absorption band at 3607 cm^{-1} was detected only when KI pellets were prepared. Furthermore, these absorption bands were not observed in the Georgia kaolinite used as reference, although kaolinites from the Georgia sedimentary deposits are known to incorporate structural Fe—in lower quantities, however, than soil (lateritic) kaolinites (Muller and Calas, 1993). The absorption band near 3600 cm^{-1} was only observed for the most disordered Fe-bearing sedimentary kaolinites studied by Brindley et al. (1986). The attribution of the 3598 and 875 cm^{-1} bands to Al-Fe^{3+}OH vibrations seems to be confirmed by studies of synthetic kaolinites formed by hydrothermal treatment of nontronite (Delvaux et al., 1989) and by hydrothermal aging of Fe^{3+} doped gels (Petit and Decarreau, 1990). However, Petit and Decarreau (1990) did not find these bands in the hydrothermal GB3 sample used as reference, although it contains structural Fe as shown by an EPR study (Angel and Vincent, 1978). Furthermore, the most iron-rich synthetic kaolinites exhibited a large band at 3535 cm^{-1}, associated with a shoulder at 820 cm^{-1}, which (by analogy with Fe-bearing micas) were assigned to Fe^{3+}–OH–Fe^{3+} stretching and deformation vibrations, respectively (Petit and Decarreau, 1990).

Table 1. Sources, mineralogy and total Fe content (before and after DCB treatment) of kaolinite samples.

Provenance	Sample name	Mineralogy[1] (CDB samples)	% Fe_2O_3[2] "raw"	% Fe_2O_3[2] "DCB"
Charentes, France = WHOLE BASIN	BCH3	Kt, Il, Qz	1.20	1.20
	BCH5	Kt, Il, Qz	1.02	0.99
	BCH6	Kt, Il, Qz	1.22	1.10
	BDG3	Kt, Il, Qz	2.56	1.45
	BDG4	Kt, Il, Qz	1.42	1.37
	CHA2	Kt, Il, Qz	0.72	0.70
	CHA5	Kt, Qz	0.73	0.74
	FBT2	Kt, Qz, At	1.05	0.83
	FBT4	Kt, Qz, At	1.45	1.22
	LAP1	Kt, Gb	0.70	0.66
	LAP3	Kt, Il, Qz	1.14	1.14
	LSB3	Kt, Il, Qz	2.31	2.11
	LSB5	Kt, Il, Qz	2.06	2.02
	LTP3	Kt, Il, Qz	2.40	1.64
	LTP5	Kt, Il, Qz	1.54	1.48
	LTP6	Kt, Il, Qz	3.75	1.82
	PDP1	Kt, Gb	0.53	0.43
	PDP2	Kt, Gb	0.43	0.36
	PDP3	Kt, Gb	0.27	0.23
	SGN2	Kt, Il, Qz	1.09	1.04
	SGN3	Kt, Il, Qz	1.17	1.17
Charentes France = Local sampling on FBT open-pit (Fontbouillant)	FBT2A-01	Kt, Qz, At	1.23	0.56
	FBT2A-02	Kt, Qz, At	1.02	0.75
	FBT2A-03	Kt, Qz, At	0.93	0.75
	FBT3A-04	Kt, Qz, At	1.09	0.97
	FBT4A-05	Kt, Qz, At	1.16	1.03
	FBT5A-09	Kt, Qz, At	3.15	1.73
Charentes (Fontbouillant)	FU7	Kt, Qz, At	0.98	0.79
Georgia, USA	US2	Kt, Gb	0.23	0.22
	US3	Kt, Qz, At	1.01	0.86
Cornwall, Great Britain	GB3	Kt, Ms, Qz	0.79	0.68
	Dinky A83	Kt, Ms, Qz	0.55	0.53
Britanny, France	FCF	Kt, Ms, Qz	0.40	0.33
Goyoum, Cameroun = SOILS KAOLINS	KD	Kt, Qz	6.53	1.32
	JZ	Kt, Ms, Qz	0.65	0.53
	PO	Kt, Ms, Qz	8.11	0.91
	OB	Kt, Ms, Qz	11.60	1.25
	JU	Kt, Ms, Qz	29.30	0.48
	GM	Kt, Ms, Qz	11.10	1.03
	NI	Kt, Qz, Gb, Ms	11.30	1.70
	GC	Kt, Ms, Ms	11.30	1.28

[1] Kt = kaolinite, Il = illite, Ms = muscovite, Qz = quartz, Gb = gibbsite, At = anatase.
[2] Fe content determined by chemical attack on raw and DCB-treated samples.

FTIR investigations of kaolinite have been carried out in order to elucidate the relationships between structural Fe and specific features on IR spectra. In contrast with previous studies, the present paper 1) deals with a wide range of kaolinites from different environments and with varying particle size and degrees of disorder; 2) uses a Fourier-transform IR spectrometer that yields information in both the mid- (600–4000 cm^{-1}) and the near-infrared (4000–10,000 cm^{-1}) regions; and 3) combines IR and EPR data to validate the assignment of IR bands related to the presence of structural Fe. It, thus, allows a quantitative comparison of Fe-content in kaolinites from various origins. A new absorption band can be identified for use in studying the variation of Fe-content in the structure of any natural kaolinite.

EXPERIMENTAL METHODS

Materials

Kaolinites from several origins were investigated: sedimentary kaolinites from late Cretaceous and Tertiary formations; soil kaolinites; and hydrothermal kaolinites. Table 1 lists the source, mineralogy, and total Fe-content of the samples studied, determined before and after the complexing dithionite-citrate-carbonate (DCB) treatment. The sample abbreviations listed in this table are used throughout the paper.

Sedimentary kaolinites. Most of the sedimentary kaolinites come from the Charentes sedimentary basin (France). They were extracted from kaolins mined in the western part of the Charentes kaolin district which

Table 2. IR and EPR (low temperature) area measurements (values in arbitrary units), specific surface areas (BET) and P2 cristallinity indices of kaolinites samples.

Sample name	EPR (a.u.) [Fe(I)] ("peak ratio")	EPR (a.u.) [Fe(II)] ("peak ratio")	[Fe(II)] (g = 9)	Area of the 4465 cm^{-1} IR band	Specific surf. area (m^2/g)	Index P2
BCH3	27.6	351	—	79.2	20.7	0.982
BCH5	29.5	352	—	82.1	24.9	0.933
BCH6	24	316	—	79.3	24.8	0.961
BDG3	23.8	359	—	94.2	28.6	0.996
BDG4	28	420	—	106	21.7	0.995
CHA2	16.6	170	—	16	30.2	0.894
CHA5	13.9	234	154.6	44.9	19	0.886
FBT2	36.2	167	114.9	4	61	0.876
FBT4	57.6	230	165.2	20	73.4	0.9
LAP1	12.7	158	95.2	25	28.6	1.016
LAP3	22.7	320	—	59.3	16.1	0.998
LSB3	36.2	399	—	127.7	2.62	0.971
LSB5	34.3	390	—	146.4	23.3	0.974
LTP3	35.8	415	232.5	123.2	23.5	0.971
LTP5	29.8	386	—	125.2	23.4	0.985
LTP6	33.6	400	—	124	26	0.979
PDP1	6.4	98	—	13	20.1	0.959
PDP2	5.4	107	—	17	20.5	0.903
PDP3	3.9	43	28.9	11.3	21.5	1.061
SGN2	28	396	—	81.3	26.1	0.972
SGN3	24	390	—	86.5	20.3	0.995
FBT2A-01	27.8	127	84.4	4.1	35.3	0.873
FBT2A-02	49.3	215	136	4.6	53.9	0.87
FBT2A-03	51	240	148.4	4.7	61.7	0.86
FBT3A-04	61.2	243	176	8	69.8	0.868
FBT4A-05	72.6	283	193.3	11.4	75.2	0.864
FBT5A-09	90.2	365	186	72.8	54.9	0.861
FU7	42.7	208	124.7	8.5	52.3	0.87
US2	5.5	64	41.5	14.9	12.5	0.973
US3	21.8	360	217.6	72	18.6	0.933
GB3	8	350	200	52	11.8	1.047
Dinky A83	12	170	—	31	13.6	1.083
FCF	8.1	161	93.1	26.7	18.5	1.073
KD	16.3	450	231.8	134.6	13.9	1.113
JZ	12.9	158	73	15.3	2.6	0.974
PO	8.9	306	155.4	57	15.7	1.072
OB	16.1	477.6	255	83	20.8	1.042
JU	8.3	94	43.4	10.4	29.3	1.06
GM	20	469	242	66.9	10	1.047
NI	70.5	362	270	41.7	53	0.903
GC	50.7	297	221.6	36.6	41.5	0.916

belongs to a Tertiary paleo-deltaïc network (Dubreuilh *et al.*, 1984). Postsedimentary evolution generated gibbsite and ordered kaolinite in some parts of the basin (Dubreuilh *et al.*, 1984). Twenty-one samples were selected from a study of the whole basin (Delineau *et al.*, 1992). Each sample is represented by three letters indicating the name of the open-pit and a number indicating its position. This general sampling was complemented by a more restricted one (in the FBT open-pit (Fontbouillant)), which allowed us to study in detail very poorly crystallized kaolinites (FBT 2A to 5A).

Data from chemical, thermal (gravimetric and differential), X-ray diffraction, and microprobe analyses have been presented elsewhere (Yvon *et al.*, 1982; Delineau *et al.*, 1992). They showed that the raw material contains 80–95 wt. % of kaolinite, except the PDP2 sample, which contains only 50 wt. % of kaolinite only. Major impurities are illite (less than 10 wt. %), quartz, hematite and goethite, sulphides such as pyrite and their weathering products, locally abundant gibbsite (45 wt. % in sample PDP2), and traces of smectites and interlayered clay minerals (Table 1). FBT Samples are illite- and smectite-free and are characterized by very disordered kaolinites with high specific surface areas (35–75 m^2/g). Only the fractions smaller than 40 μm in diameter, obtained after sieving, were used for this study.

Three other sedimentary reference kaolinites (Cases *et al.*, 1982) were also investigated: US2, US3 (Georgia deposit, Huber Corporation), and FU7 (Charentes deposit, Argiles et Minéraux-AGS), sampled in the FBT open-pit in 1973.

Soil kaolinites. Soil kaolinites were sampled in laterites from Goyoum, East Cameroon. Weathering profiles were developed on a gneissic basement under permanently humid conditions and forest cover (Muller and Bocquier, 1986, 1987; Muller, 1988; Muller and Calas, 1989; Braun *et al.*, 1990). The selected samples represent a large range of degree of disorder (Muller and Bocquier, 1987) and of Fe-content in different sites (Muller and Calas, 1993). Apart from kaolinite, a $2M_1$-muscovite is the only other Fe-bearing phyllosilicate found in these kaolins (Muller, 1988). The mineralogical composition deduced from XRD diffractrograms on CDB treated samples, shows that PO, OB, GM, JU, and JZ contain muscovite (25–30 wt. %), kaolinite (50–55 wt. %) and quartz (20–25 wt. %), whereas NI, GC and KD contain kaolinite (60–70 wt. %), minor amounts of muscovite (<5 wt. %), and quartz (20–30 wt. %). GC also contains small amounts of gibbsite (<5 wt. %). NI and GC are poorly ordered and exhibit high specific surface areas (Table 2).

Hydrothermal kaolinites. Three standard commercial grade hydrothermal kaolins, were used in this study: GB3 and Dinky A83 are well-ordered primary, granite-hosted kaolinites from the Cornubian ore field of southwest England (English China Clay, St. Austell, Cornwall: Jackson *et al.*, 1989). FCF is also granite-hosted kaolinite; it comes from the Berrien ore of Brittany (Société de la Cornouaille Française, Finistère, France). Detailed mineralogical and chemical analyses of these samples have been presented previously (Liétard, 1977; Cases *et al.*, 1982, 1986).

Fourier-transform infrared spectroscopy

IR spectra were obtained on a Bruker IFS 88 Fourier-transform infrared (FTIR) spectrometer. Three different detectors were used to optimize the spectrometer in the spectral ranges 600–4000 cm^{-1} (mid-infrared,

MIR) and 4000–10,000 cm^{-1} (near-infrared, NIR) in both diffuse reflectance and transmission modes.

MIR–diffuse reflectance. The spectrometer was equipped with a large band mercury-cadmium-telluride (MCT) detector cooled at 77 K. The diffuse reflectance attachment was manufactured by Harrick Scientific Corporation. About 70 mg of air-dried sample was mixed with 370 mg of ground KBr in order to avoid signal saturation. The samples were packed loosely into a sample cup (depth 3 mm, diameter 9 mm) to achieve a nearly random orientation. The sample area measured by the spectrometer was about 1 cm by 0.5 mm. Two hundred scans at a resolution of 4 or 1 cm^{-1} were averaged. The absorbance unit used corresponds to the decimal logarithm of the ratio:

$$\frac{\text{reflectance of the pure finely powdered KBr used as a reference}}{\text{reflectance of the sample}}$$

The same unit was used for the NIR. The reference spectrum of atmospheric water was always subtracted. For comparison purposes, all spectra were normalized by reference to the Si–O vibration band (1100 cm^{-1}) of kaolinite.

NIR–diffuse reflectance. The spectrometer was equipped with a liquid nitrogen cooled Indium Antimony (InSb) detector. Two hundred scans at a resolution of 4 cm^{-1} were signal averaged. Samples were analyzed without any dilution in KBr. Most of the spectra were recorded at room temperature, some under vaccum (10^{-2} Pa). As absorption bands in the NIR region are Al or Fe dependent, normalization of band intensities was impossible as far as Fe for Al substitution was concerned. The intensity of the absorbance peaks was measured from a tangentially drawn baseline.

Transmission spectroscopy. Because the Hinckley index does not estimate the types or abundances of various structural defects (the classical "crystallinity," Plançon *et al.*, 1988), the structural order of the kaolinite samples was estimated from transmission spectroscopy data in the MIR domain. There is a quantitative relation between the relative intensities of the bands at 3669 and 3650 cm^{-1}, determined after baseline correction, and the crystallographical order of kaolinite (Cases *et al.*, 1982). A "disorder index" P_2 can then be defined as the ratio of the apparent intensities of these two bands which, according to previous observations on sedimentary kaolinites (Cases *et al.*, 1982), soil kaolinites (Muller and Bocquier, 1987), and hydrothermal kaolinites (Muller *et al.*, 1990), increases with increasing degree of order.

In the MIR domain, the spectrometer was equipped with a deuterated triglycine sulphide (DTGS) detector, and the spectral resolution was 1 cm^{-1}. In the near infrared (NIR), the InSb detector was used with a 4 cm^{-1} spectral resolution. The pressed KBr pellet technique was used. A mixture of 2 or 20 mg of sample (respectively, for MIR and NIR experiments) and 148 mg of KBr was gently stirred for about 1 min by a pestle in a mortar without exerting any pressure that could disorder the clay material. This mixture was placed in a pellet die and pressed under vacuum at 15,000 kg total pressure. The resulting pellet, 13 mm in diameter and approximately 150 μm in thickness, was uniformly transparent to the eye. The values obtained for the P_2 index, determined after DCB treatment (see below), are reported in Table 2.

Electron paramagnetic resonance

EPR spectroscopy has been described in several reviews (e.g., Calas, 1988). X-band (~9.2 GHz) EPR spectra were registered using a CSE 109 Varian spectrometer. The experimental parameters were the following: 100 kHz modulation frequency, 3.2 G modulation amplitude, and a time constant of 0.125 s. A 40 mW microwave power was chosen because of the absence of EPR signal saturation. EPR spectra were recorded at room temperature and at 93 K using a liquid nitrogen cooled cavity. The lower temperature allowed a strong enhancement of the Fe^{3+} spectral intensity with respect to the background spectra due to residual superparamagnetic iron-oxides (Bonnin *et al.*, 1982).

The observed EPR signals were labeled by their g values, g_{eff} being defined by the relation $h\nu = g_{eff}\beta B$, where h is Planck's constant; ν is the resonance frequency; g is the electronic "factor", i.e., a tensor of second rank with the eigenvalues g_{xx}, g_{yy}, g_{zz}; B is the field at which resonance occurs; and β is the Bohr magneton. The g-values were calibrated by comparison with a standard (DPPH: 1,1-diphenyl-2-picrylhydrazyl; $g_{DPPH} = 2.0037 \pm 0.0002$). The error in g-value measurement was estimated to be ± 0.001. The accuracy on magnetic field values was $\Delta B = \pm 1$ G. A 4 mm diameter pure silica tube (Suprasil grade) was filled at a constant height (15 mm) for each weighed sample (about 40 mg).

A strong perturbation arose from the presence of Fe oxides, which are always associated with natural kaolinites. These oxides (occuring either as distinct phases or coatings) are responsible for a broad resonance ($\Delta B > 1000$ G), which superimposes on the EPR signal of structural Fe (Angel and Vincent, 1978, Bonnin *et al.*, 1982). Fe oxides have, thus, been eliminated using the complexing DCB method (Mehra and Jackson, 1960) carried out at 80°C. The total Fe contents measured before and after the DCB treatment are listed in Table 1. It was verified, after Muller and Calas (1989), that the DCB treatment does not influence the kaolinite structure nor the shape and intensity of the spectra corresponding to structural Fe. However, the Fe oxides cannot be removed totally, particularly in soil samples

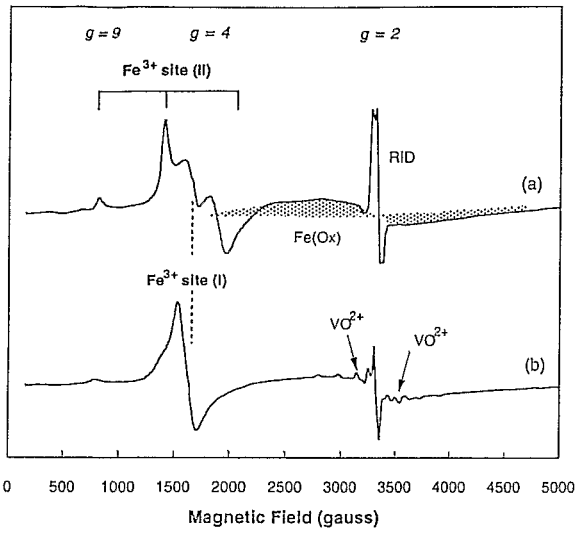

Figure 1. Typical full range X-band EPR spectra (recorded at room temperature, after deferrification treatment) of: a) a poorly crystallized sedimentary kaolinite from Charentes, France (FBT2A-02); and b) a well-crystallized hydrothermal kaolinite from St Austell, England (GB3).

(Herbillon *et al.*, 1976; Muller and Calas, 1989). Even if its intensity is reduced at low temperature, a weak broad isotropic resonance remains due to residual superparamagnetic Fe oxide species (Muller and Calas, 1993). For most samples, spectroscopic analyses were carried out before and after the deferration treatment. EPR measurements listed on Table 2 refer to DCB treated kaolins, except for reference kaolinites and locally sampled FBT kaolinites.

As the samples investigated had the same kind of centers, EPR spectra presented a similar shape. Therefore, the concentration of the paramagnetic centers could be estimated by using a simplified procedure (Calas, 1988). Since the experimental parameters are held constant, the concentration of paramagnetic centers can be assumed to be proportional to $S = \Delta B^2 I / ga \cdot m$, where ΔB is the linewidth peak-to-peak, I the signal intensity, ga the gain, and m the sample weight. This "peak ratio" procedure yielded an estimate, in arbitrary units, of the relative concentration of ferric iron in two distinct sites (Mestdagh *et al.*, 1980; Muller *et al.*, 1990; Muller and Calas, 1993).

Specific surface area measurements

The specific surface areas of the non deferrated samples were determined by the BET method using nitrogen as adsorbing gas. The data are reported in Table 2.

RESULTS AND DISCUSSION

EPR spectroscopy

Paramagnetic species encountered. Two overall X-band EPR spectra of representative kaolin samples recorded at room temperature are presented in Figure 1. They show most of the resonances that have been described for natural kaolins (Jones *et al.*, 1974; Meads and Malden, 1975; Hall, 1980; Muller and Calas, 1993).

A complex EPR signal arises, at low magnetic field ($g = 4$ region) from Fe^{3+} in two distinct sites (Brindley *et al.*, 1986) referred to here as Fe(I) and Fe(II) sites. Although they both correspond to Fe^{3+} ions substituted in the octahedral layer of kaolinite, they are distinguished by the type of site distortion: 1) Fe(I) sites correspond to rhombically distorted sites and give rise to a nearly isotropic signal centered at $g = 4.3$; and 2) Fe(II) sites show a slight axial component and give rise to a superimposed anisotropic signal with g-values at 9, 4.9, 3.7, and 3.5. While the latter have been demonstrated to arise from Fe^{3+} substituted for Al^{3+} at the two octahedral positions inside the XRD-coherent domains (Gaite *et al.*, 1993), the former are thought to be located at the boundary of these domains (Muller and Calas, 1993) and are connected with heterogeneities that destroy the regular pattern of the kaolinite crystal (Mestdagh *et al.*, 1980).

The resonances observed at high magnetic field ($g = 2$ region) represent an overlay of: 1) a broad resonance ($\Delta B > 1000$ G) due to superparamagnetic Fe oxyhydroxides (Fe(Ox) on Figure 1a); 2) a sharp, intense signal due to positive holes trapped on oxygen atoms, which have been demonstrated to be radiation-induced defects (RID on Figure 1a) (Muller *et al.*, 1990); and 3) a weaker eight-line hyperfine structure that appears for sedimentary kaolinites (Figure 1b) and that is due to VO^{2+} ions trapped within kaolinite particles (Muller and Calas, 1993).

The intensity of the different signals, thus the concentration of corresponding paramagnetic species, can vary greatly from one sample to another. Particularly, and as exemplified on Figure 1, the relative intensity of signals due to structural Fe in Fe(I) and Fe(II) sites can exhibit a wide range of variation among the samples.

Variation of Fe^{3+} distribution in the kaolinite structure. The concentrations of trivalent iron in Fe(I) and Fe(II) sites, referred to here as [Fe(I)] and [Fe(II)], are listed in Table 2. The relative error in area measurements were evaluated to be 10% for [Fe(I)] and 10% to 20% for [Fe(II)], depending on the resolution of the signal of Fe(II) (Allard *et al.*, 1992). Figure 2 illustrates the variations of [Fe(II)] as a function of [Fe(I)] for the kaolinites from the three different environments. Figure 2a shows that [Fe(I)] and [Fe(II)] measured for sedimentary kaolinites from the Charentes basin have a similar ratio of [Fe(I)] to [Fe(II)]. Samples are grouped in two ways according to their origin: by structural order and specific surface area. The ordered kaolinites (high P_2 index) from the whole sedimentary basin with a medium specific surface area (10 to 28 m^2/g), present

the highest amount of iron in Fe(II) sites. The highly disordered kaolinites with high specific surface areas, sampled mainly in the FBT site, are characterized by the highest content of iron in Fe(I) sites (Table 2). The observed relation between [Fe(I)] and [Fe(II)] confirms the previous data of Allard *et al.* (1992). It suggests a change in Fe partition during a post-sedimentation recrystallization process. By contrast, Figure 2b shows that [Fe(I)] and [Fe(II)] for soil, hydrothermal, and other sedimentary kaolinites are almost independent.

Impurity effects on EPR spectra of structural iron. Gibbsite, illite or muscovite, smectite, and chlorite, i.e., the main Fe-bearing phyllosilicates present as impurities in the studied kaolinitic materials, can contribute to the EPR spectra of structural Fe (Jones *et al.*, 1974; Kemp, 1973; Olivier *et al.*, 1975; Hall, 1980). This possibility was, therefore, evaluated. The gibbsite contribution can be neglected because of the low content of gibbsite in most samples (<3 wt. %), or the very low Fe content (lower than the detection limit) in gibbsite from the most enriched samples (e.g., 45 wt. % of gibbsite in PDP2), as shown by quantitative microprobe analysis (Delineau *et al.*, 1992). Illite or muscovite could contribute mainly to the Fe(I) signal and secondarily to the Fe(II) signal. However, this contribution is negligible for sedimentary and hydrothermal kaolins because of their low content in 10 Å-phases (<10 wt. %). Furthermore, it has been shown that even if the muscovite content can be as high as 20 to 30 wt. % in lateritic soils, the presence of this impurity has a weak influence on the EPR spectra of kaolinities (Muller, 1988). It only gives rise to a slight overestimation of [Fe(II)] determined by the peak ratio method. Since smectite and chlorite abundances are near the limit of detection by XRD, their influence on EPR spectra of structural Fe can be considered as negligible.

The large resonance centered at $g = 2$, due to occluded superparamagnetic Fe oxyhydroxides that resisted the deferration treatment, is partly superimposed on the spectrum of structural Fe in kaolinite (Bonnin *et al.*, 1982). This resonance is largest for soil samples (Muller and Calas, 1989). This could result in an underevaluation of the area of the signal and, thus, of the concentration in structural Fe (see Figure 1a: the signal due to Fe-oxyhydroxides disminishes the absolute intensity of the Fe(II) peak near 1900 Gauss). Furthermore, Fe(II) content can be further underestimated, particularly for the most disordered kaolinites (Muller and Bocquier, 1987, and Figure 1b), because the intensity of Fe(I) signal is greater than that of the Fe(II) signal. In order to evaluate the extent of possible underestimation of the area of the Fe(II) signal by the peak ratio method, the previously mentioned S parameter was compared to the area of the only $g = 9$ component, which is also related to [Fe(II)] (Meads and Malden, 1975) but is weakly affected by the overlay of

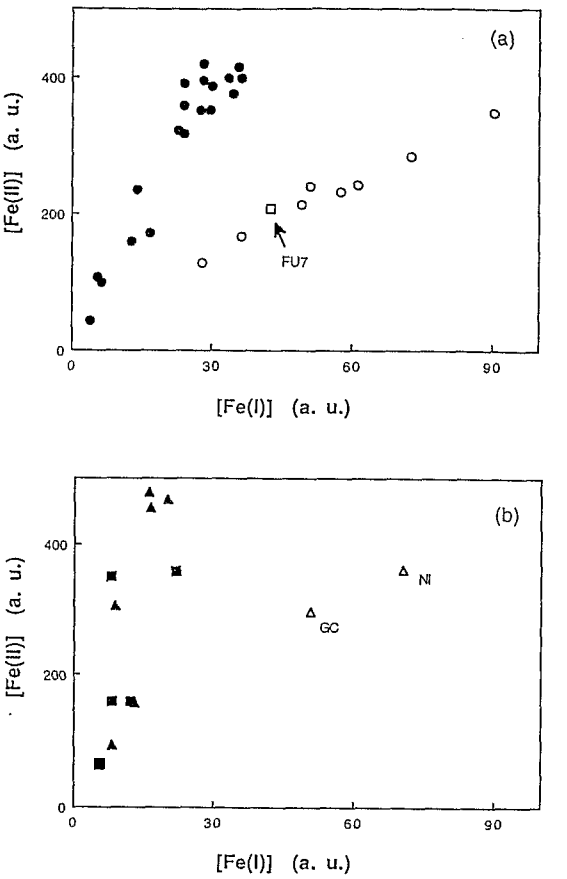

Figure 2. Plots of concentration, expressed in arbitrary units (a. u.), of substituted-Fe^{3+} in Fe(I) and Fe(II) sites: a) sedimentary kaolinites from Charentes basin (full circles = from the whole basin, excluding FBT local site; open circles and open square = from the FBT local site); b) soil kaolinites (open and full triangles) and standard hydrothermal and sedimentary kaolinites, except FU7 (full squares).

spectra from Fe(I) and residual oxyhydroxides. Figure 3 shows that these two areas are closely correlated (correlation coefficient $\rho = .992$ for the purest samples: sedimentary and hydrothermal kaolinites; and .986 for soil kaolinites). This indicates that the error inherent to the measurement of [Fe(II)] by the peak ratio method is low with respect to the total variation of the content of structural Fe among the samples. Therefore, this method can be considered as suitable for comparing the samples. For the samples GM, OB, PO, JZ, and JU, the slight overestimation of [Fe(II)] measured using the peak ratio method (Figure 3), in comparison with sedimentary and reference kaolinites, is due, as explained above, to the influence of muscovite. The influence of overlay from Fe(I) and residual oxyhydroxides probably lead to an underestimation of [Fe(II)] measured with peak ratio method for the samples GC and NI. Figure 3 shows that the highest [Fe(II)] values are obtained for soil samples KD, OB, and GM. The

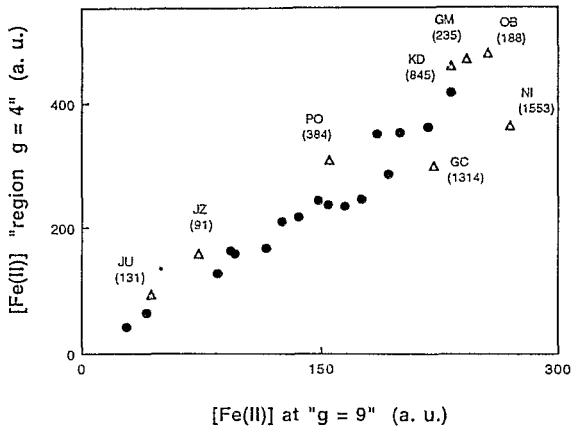

Figure 3. Plot of substituted Fe^{3+} in Fe(II) sites, expressed in arbitrary units (a. u.), determined according to two procedures: 1) measurement according to the classical peak ratio method (EPR signal in the $g = 4$ region: Muller *et al.*, 1990); and 2) measurement of the area of the $g = 9$ resonance. Full circles = sedimentary kaolinites from Charentes and reference kaolinites. Open triangles = soil kaolinites. Concentration (in arbitrary units) of occluded superparamagnetic oxyhydroxides (Fe(Ox) on EPR signal) are indicated in brackets for the soil samples.

relatively low amount of kaolinite in soil samples (in comparison with sedimentary and hydrothermal kaolinites) indicates that the kaolinite of these samples contains much more substituted Fe than kaolinites from the two other environments.

Infrared reflectance spectroscopy

MIR spectra. Figure 4 presents the FTIR diffuse reflectance spectra, in the range 3400–3750 cm^{-1}, of representative kaolinites containing variable amounts of structural Fe (e.g., [Fe(II)] increasing from 43 a. u. for PDP3 to 456 a. u. for KD). Except for the Fe-poor PDP3 kaolinite, an absorption band at 3598 cm^{-1} is systematically observed as a shoulder on the low wavenumber side of the OH-stretching vibration band. Furthermore, expanded spectra (not shown) reveal that this band broadens with increasing degrees of disorder (i.e., P_2 index decreases, in Table 2). No band was observed at 3535 cm^{-1}, but some spectra (e.g., KD, in Figure 4) exhibit a band at 3435 cm^{-1} that was not modified under vacuum at 10^{-2} Pa and disappeared after heating at 300°C. This band was observed earlier on synthetic kaolinites (Petit and Decarreau, 1990) and natural disordered kaolinites (Kato *et al.*, 1977) but has not been assigned.

Absorption bands in the 750–1200 cm^{-1} region for some of the kaolinites are presented in Figure 5. A shoulder at 875 cm^{-1} is systematically present. Another small shoulder at about 830 cm^{-1} is also present in the samples containing more than about 5 wt. % of illite or muscovite impurities (samples GM and GB3

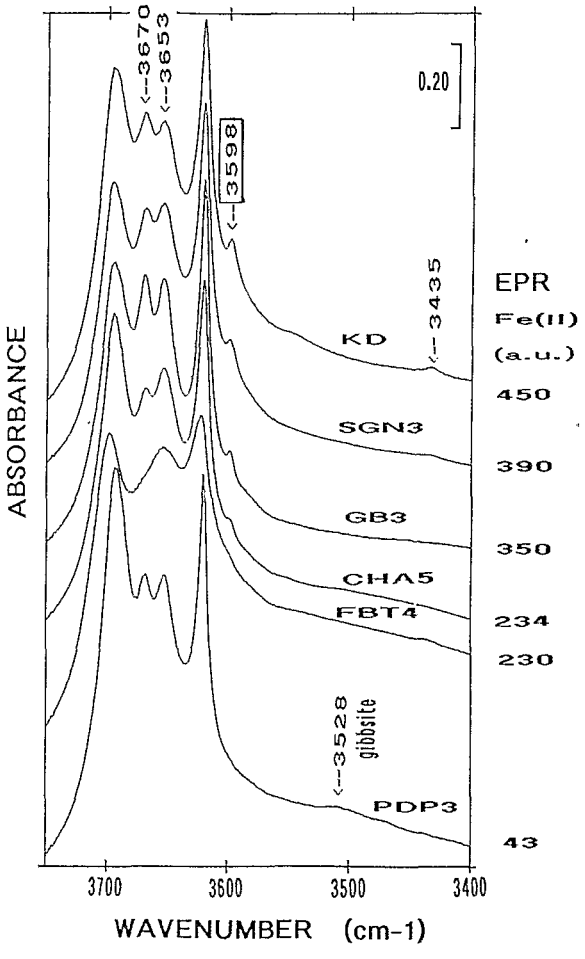

Figure 4. Diffuse reflectance IR spectra in the 3400–3750 cm^{-1} region for selected samples containing variable amounts of substituted Fe^{3+} in Fe(II) sites ([Fe(II)], expressed in arbitrary units (a. u.).

in Figure 5). This band is likely due to the OH deformation mode of the Mg–OH–Al bond in micas (Fripiat and van Olphen, 1979).

It must be pointed out that most spectra obtained in transmission also exhibit the two shoulders near 3600 and 875 cm^{-1} present in diffuse reflectance spectra. However, because of their lower intensity, they are most apparent only for kaolinites containing the highest amount of structural Fe, i.e., the soil kaolinities and some sedimentary kaolinities. The higher sensitivity of diffuse reflectance (associated with a high resolution power: 1 cm^{-1}) is clearly demonstrated by considering the GB3 spectra. Although the band at 3598 cm^{-1} was not observed in spectra obtained in the transmission mode (Petit and Decarreau, 1990), it is clearly present in diffuse reflectance spectrum (Figure 4).

The presence of absorption bands at 3598 and 875 cm^{-1} in each of the natural kaolinites studied (except PDP3) and the parallel increase of their intensity with

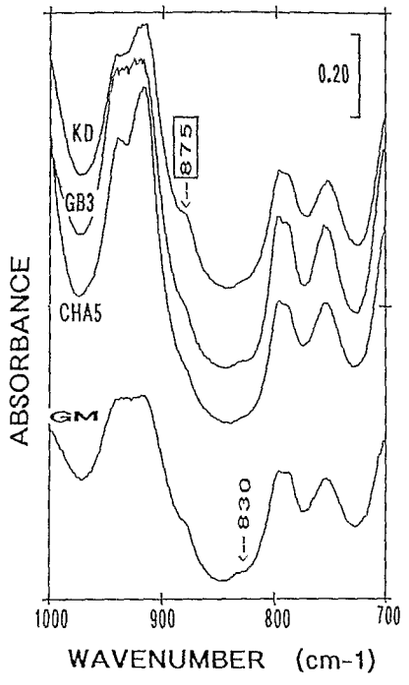

Figure 5. Diffuse reflectance IR spectra in the 700–1200 cm^{-1} region for selected samples containing variable amounts of substituted Fe^{3+} in Fe(II) sites. The band at 830 cm^{-1} is only observed for samples containing more than 5% of muscovite or illite impurity (25% in GM soil sample; 10% in GB3).

the content of structural Fe in the Fe(II) site seems to confirm the assignment of these two bands to Al-Fe^{3+}OH vibrations. However, because of their weak intensity and their position, a quantitative appraisal cannot be achieved.

NIR spectra. Major NIR spectral features of silicate minerals are located in the 4000–5500 cm^{-1} and 6500–7500 cm^{-1} domains (Hunt and Salisbury, 1970; Hunt, 1977). The observed signals correspond to the first harmonic of OH stretching fundamental vibration modes, to combinations of stretching and deformation fundamental modes in X–OH groups (X = Al, Mg, or Fe mainly), or to combinations of OH stretching fundamental modes with lattice vibrations.

Diffuse reflectance spectra of the selected kaolinites in the 4000–5500 cm^{-1} domain are presented on Figure 6. The major band at 4528 cm^{-1} and the associated one at 4620 cm^{-1} can be assigned by reference to spectra presented previously (Hunt and Salisbury, 1970; Hunt, 1977). They correspond to the combination of OH stretching and deformation modes of Al–OH–Al groups. The weaker band near 4730 cm^{-1} is likely due to a combination of the internal OH elongation (3620 cm^{-1}) with lattice vibration (Si–O stretching near 1110 cm^{-1}). The three little bands between 4100 and 4300 cm^{-1} are probably combinations of OH stretching bands

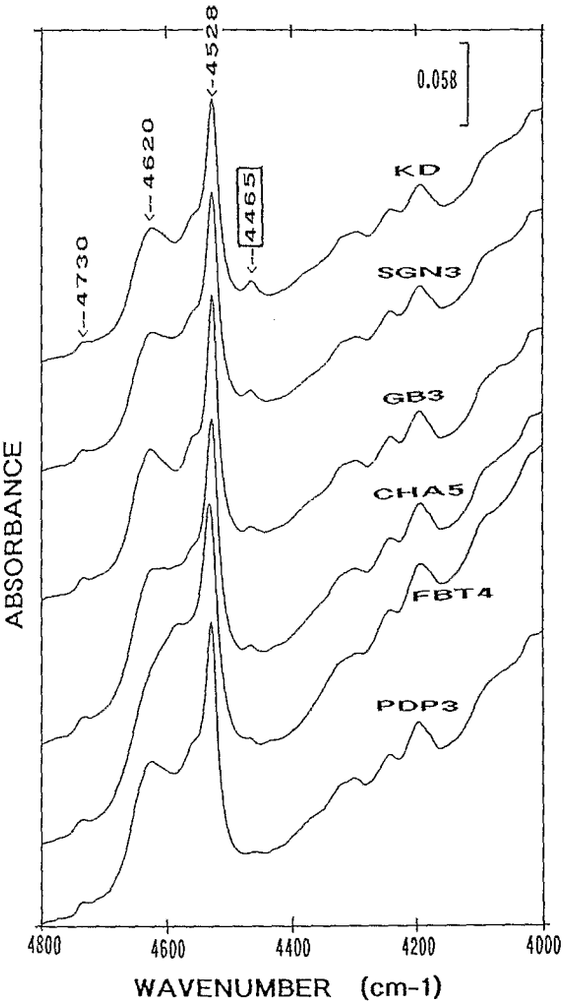

Figure 6. Diffuse reflectance NIR spectra in the 4000–5500 cm^{-1} region of the samples presented in Figure 4.

of kaolinite with lattice deformation vibrations. A diagnostic band of adsorbed water, close to 5263 cm^{-1} (Hunt, 1977), is only observed in spectra recorded at ambient atmosphere, and it disappears under vacuum (not shown).

An additional band at 4465 cm^{-1} was systematically observed for all the natural kaolinites. The intensity of this band increases with that of the bands at 3598 and 875 cm^{-1} (Figures 4 and 5, respectively). This band at 4465 cm^{-1} has never been mentioned in the literature and can logically be assigned to the combination of the 3598 and 875 cm^{-1} bands observed in the medium-infrared spectra. For the more ordered samples (US2, PDP3, LAP1, DinkyA83, GB3, and JU), the absorption band at 4465 cm^{-1} appears to be composed of two bands near 4467 and 4458 cm^{-1} (for example, sample US2 on Figure 7c). By analogy with Al–OH–Al vibrations, this could be due to a distinction between

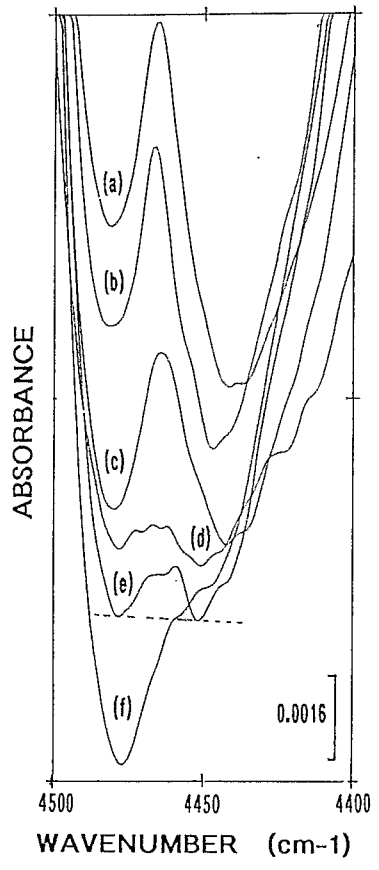

Figure 7. Expanded version of the absorption band at 4465 cm^{-1} for selected samples: a) soil sample (OB) containing 25% of muscovite; b) Georgia sedimentary kaolinite (US3) without illite and gibbsite impurities; c) soil sample (PO) containing 25% of muscovite; d) Highly disordered Charentes sedimentary kaolinite (without illite) (FU7); e) US2 kaolinite after heating at 300°C for 2 h; and f) Low-iron and gibbsite-containing (0.22 wt. % Fe_2O_3; 1.5 wt. % gibbsite) Georgia sedimentary kaolinite (US2). ----- = baseline for sample e.

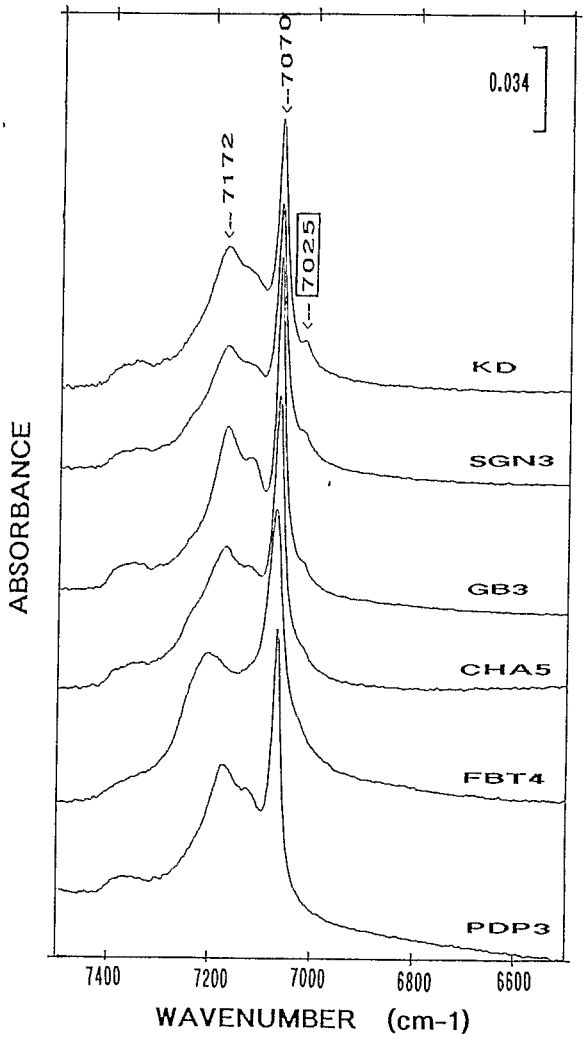

Figure 8. Diffuse reflectance NIR spectra in the 5500–7500 cm^{-1} region of the samples presented in Figures 4 and 6.

internal and external OH (Ledoux and White, 1962) of the elementary sheet of kaolinite.

Diffuse reflectance spectra in the 6500 to 7500 cm^{-1} domain are presented on Figure 8. The major band at 7070 cm^{-1} and the associated one with lower intensity at 7172 cm^{-1} can be also assigned by reference to spectra presented by Hunt and Salisbury (1970) and Hunt (1977). They correspond to the first harmonics of OH elongation fundamental modes of Al–OH–Al groups. Again, the only difference with spectra presented in the literature is the presence of a weak band centered near 7025 cm^{-1}, which appears as a shoulder on the major band at 7070 cm^{-1}. This band, which does not disappear under vacuum, likely corresponds to the first harmonic of the 3598 cm^{-1} band. Furthermore the intensity increase of the band at 7025 cm^{-1} also parallels that of the bands at 3598 and 875 cm^{-1}, i.e., it is not observed for PDP3, while it is the most intense for KD. This confirms the assignment of this band. As observed for MIR spectra, the bands at 4465 cm^{-1} and 7025 cm^{-1} are also present in most of the spectra recorded through the transmission mode, but they are markedly less intense.

Area of the band at 4465 cm^{-1}

Four absorption bands in the diffuse reflectance spectra, located at 875, 3598, 4465, and 7025 cm^{-1}, seem related to the presence of trivalent Fe within the kaolinite structure. The band at 4465 cm^{-1} is best resolved in the FTIR spectra, is always the most intense, and appears even for the Fe-poor kaolinites (e.g., PDP3, in Table 2 and Figure 6). It, thus, seems to be the most convenient for establishing a quantitative relationship between FTIR measurements and Fe content of the two substitution sites measured by EPR. As shown in Figure 7, the area can be easily determined by planim-

etry of expanded spectra, a straight line joining the minima near 4445 and 4480 cm^{-1} approximating the baseline (example in Figure 7e). However, it must be pointed out that the 4528 cm^{-1} major band slightly overlaps the 4465 cm^{-1} band on its high wavenumber side (Figures 6 and 7a–7e). This overlapping increases with 1) increasing structural Fe content (increase of the intensity of the 4465 cm^{-1} band relatively to that of the 4528 cm^{-1} band); and 2) with structural disorder (broadening of the 4528 cm^{-1} band; see sample FBT4 in Figure 6). This could result in an underestimation of the area of the 4465 cm^{-1} band. However, in the present case, as significant variations of Fe substitution are considered, this calculation method seems to be precise enough. A possible underestimation of the area due to the presence of impurities or to the small size of the kaolinite particles must also be taken into account.

Impurity effects. The IR spectrum of gibbsite presents a strong absorption band near 4400 cm^{-1} due to the combination of deformation and stretching OH bands. It is noticeable even for gibbsite contents as low as 1–2% (Figure 7f, gibbsite content in sample US2 = 1.5 wt. %). However, Figure 7e shows that the area of the 4465 cm^{-1} band due to kaolinite can be determined by heating the samples at 300°C for 2 h. This treatment transforms gibbsite while kaolinite remains stable. Therefore, all the gibbsite containing samples (LAP1, PDP1, PDP2, PDP3, US2, and GC) were submitted to this pretreatment before measuring the area of the 4465 cm^{-1} band. The loss of mass occuring during this calcination was measured for a better comparison with EPR data. Except for the PDP2 sample, the mass loss had no influence.

Another impurity effect could be due to muscovite or illite, the IR spectrum of which is characterized by a large and broad absorption band near 4540 cm^{-1} (Hunt, 1977). This could then provoke a broadening of the 4528 cm^{-1} band and then influence the 4465 cm^{-1} band on its high wavenumber side. However, the 4465 cm^{-1} band of the sample PO (25 wt. % muscovite) does not appear to be perturbed by comparison with samples US3 or US2 (no muscovite or illite) (Figures 7c, b, e, respectively). The influence of muscovite on the 4465 cm^{-1} band can then be neglected.

Particle size effect. The particle size of a sample significantly affects its reflectance spectrum. Coarse samples commonly exhibit more pronounced absorption bands than fine-grained ones (Crowley and Vergo, 1988). For low-absorbing monodisperse spherical particles, the empirical relation between the reflectance (R) at a given wave number and the diameter of the particles can be written as follows (Simmons, 1971):

$$R = \exp(-2 \cdot n \cdot (k \cdot D/3)^{1/2}) \quad (1)$$

where R is the ratio of the intensity reflected by the particles to that reflected by a perfect diffuser, n is the refractive index of the material studied, k the absorption coefficient defined according to the Beer–Lambert law, and D the diameter of the particles. When the spectra are presented in apparent absorbance units [(abs) = −log R], R varies from 0 to 1. Eq. 1 then reveals that (abs) decreases when D decreases. Thus, for a given content of structural Fe, the smaller the kaolinite particle size, or the higher the specific surface area, the lower the absorbance. Eq. 1 can also be written as:

$$(abs) = \text{constant} \cdot \sqrt{D} \quad (2)$$

In order to estimate the influence of the specific surface area, the ratio of specific surface areas measured for two kaolinite samples was considered as equal to the inverse ratio of the diameter of the average particles. The size effect for particles with high surface area can be taken into account by reference to that of kaolinites was a mean surface area of 18 m^2/g. The area of the IR band can then be multiplied by $(\sqrt{s/18})$ where s is the specific surface area of the sample. For the highest surface area observed (s = 75 m^2/g), the maximum multiplication factor can reach $\sqrt{75/18} = 2$.

Figures 9 and 10 show the results obtained by applying this correcting factor to the area of the 4465 cm^{-1} band for kaolinites with high specific surface area. Table 2 shows the uncorrected data.

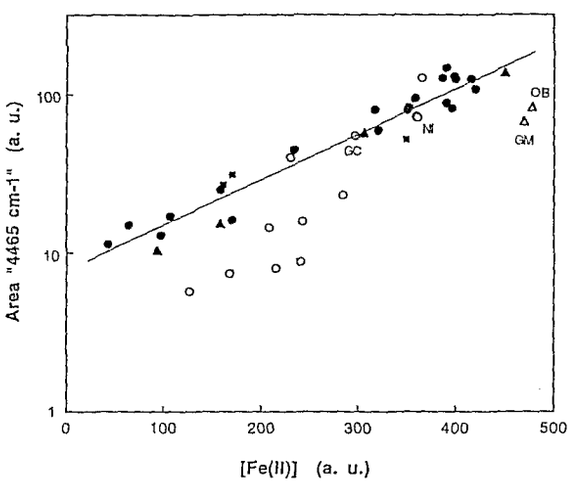

Figure 9. Semi-log plot of substituted Fe^{3+} in site II [Fe(II)] *vs.* area of the 4465 cm^{-1} diffuse reflectance NIR absorption band, expressed in arbitrary units (a. u.). Full circles = sedimentary kaolinites with low specific area. Full squares = hydrothermal kaolinites. Open circles = kaolinites with high specific surface area (Charentes FBT local site, and two soil samples NI and GC), with a size correction factor applied for these samples (see text). Open and full triangles = other soil kaolinites.

FTIR vs. EPR measurements

For most of the investigated kaolinites (full symbols on Figure 9), a general linear correlation, independent

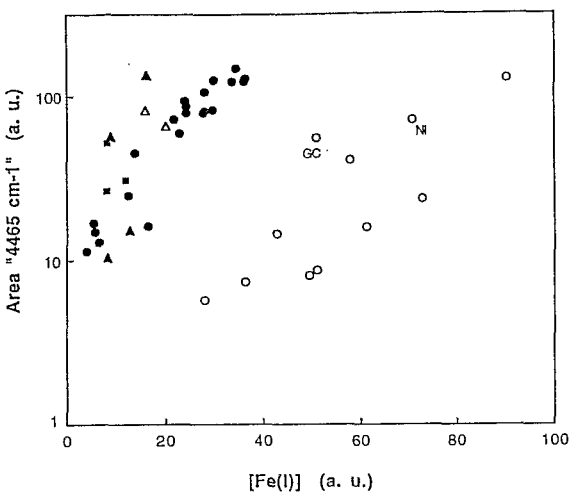

Figure 10. Semi-log plot of substituted Fe^{3+} in site I [Fe(I)] *vs.* area of the 4465 cm^{-1} diffuse reflectance NIR absorption band, expressed in arbitrary units (a. u.). Full circles = sedimentary kaolinites with low specific area. Full squares = hydrothermal kaolinites. Open circles = kaolinites with high specific surface area (Charentes FBT local site, and two soil samples NI and GC), with a size correction factor applied for these samples (see text). Full triangles = other soil kaolinites.

of the origin of kaolinites, is found between the logarithm of the area of the 4465 cm^{-1} NIR absorption band and the content of Fe^{3+} ions in site II ([Fe(II)]). The results can be expressed according to the following empirical equation:

$$\log(\text{"area 4465 cm}^{-1}\text{"}) = 0.00287 \cdot [\text{Fe(II)}] + 0.888 \quad (3)$$

The correlation coefficient ρ is equal to .968. The line drawn in Figure 9 corresponds to this equation. This relation was not so apparent for two sets of samples: the sedimentary and soil kaolinites with high specific surface area (35 to 75 m^2/g) (open circles); and the two soil kaolinites with the highest [Fe(II)] values (GM and OB). For the first set, particle size effects lead to an underestimation of the area of the 4465 cm^{-1} band. The correction factor applied (see above) really gives better results (see uncorrected data in Table 2), but seems not to be strong enough for some of these samples. Furthermore, as these kaolinites are very badly ordered, as mentioned above, the calculation of the area the 4465 cm^{-1} band is more uncertain. The major 4528 cm^{-1} strongly broadens and overlaps the high wavenumber side of the 4465 cm^{-1} band. For the second set, corresponding to the most Fe-substituted kaolinites (GM and OB), the area of the 4465 cm^{-1} band is clearly underestimated because of the influence of the 4528 cm^{-1} band (Figure 7a). In this case, better results would probably be obtained through a numerical decomposition of the IR spectra. It can thus be inferred that the 4465 and, therefore, the 3600 and 875 cm^{-1} bands correspond to diluted octahedral Fe^{3+} in the kaolinite structure.

The plot representing the variations in the area of the 4465 cm^{-1} band as a function of the concentration of Fe^{3+} ions in site I ([Fe(I)]) shows significant contrasts between different sets of samples (Figure 10). One set is composed of sedimentary kaolinites with specific surface area <35 m^2/g for which IR and EPR data are related. A second set includes samples with high specific area (>35 m^2/g) (sedimentary kaolins from FBT open pit and soil samples NI and GC) for which the area of the 4465 cm^{-1} band remains weak whatever the Fe(I) content. A third set is composed of hydrothermal kaolinites and other soil kaolinites for which no systematic relationship was observed. The relation observed for the first set (mainly sedimentary kaolinites from Charentes with medium specific surface area) is due to the fact that for these samples the ratio of [Fe(I)] to [Fe(II)] is constant (as shown above in Figure 2). In the second set of samples (kaolinites with high specific surface areas), a significant increase of the 4465 cm^{-1} band area is observed only for the highest Fe(I) contents. Particle size effects cannot be invoked for these samples as the multiplication of the area of the 4465 cm^{-1} band by 2 would lead to a poorer correlation than that obtained with [Fe(II)] in Figure 9.

It can thus be inferred that, for most kaolinites, the four absorption bands observed on the diffuse reflectance spectra and located at 875, 3598, 4465, and 7025 cm^{-1}, are mainly due to Fe^{3+} substituted for Al^{3+} at the two octahedral positions inside the XRD-coherent domains (Fe^{3+} in site II). The influence of Fe^{3+} ions in site I would be negligible, except for some very poorly ordered kaolinites which are characterized by a relatively high amount of Fe(I).

CONCLUSIONS

Major conclusions can be derived from this systematic comparative study of reflectance FTIR and EPR specra carried out on a large set of kaolins from different origins (sedimentary, soil and hydrothermal) with varying structural order and Fe content.

1) Comparisons of data obtained by means of diffuse reflectance FTIR and EPR spectroscopies provide new insight into the way structural Fe influences the IR spectra of natural kaolinites. Four absorption bands, located at 875, 3598, 4465, and 7025 cm^{-1}, are due to the presence of Fe within the crystal structure of kaolinite. This study clearly confirms the assignment of the two first bands to $AlFe^{3+}OH$ vibrations. Diffuse reflectance IR spectroscopy is a consistent tool for detecting low contents of substituted-Fe^{3+} and the sensitivity limit is probably as low as 0.2% taking into account the fact that natural kaolinites always contain both structural Fe and occluded superparamagnetic Fe-oxides. The two

bands at 4465 cm^{-1} and 7025 cm^{-1} were described for the first time. They were observed on FTIR reflectance spectra for all the samples and are attributed to the combination of the bands at 3598 and 875 cm^{-1} and to the first harmonic of the band at 3598 cm^{-1}, respectively.

2) The area of the band at 4465 cm^{-1} quantitatively correlates with the area of EPR signals due to Fe^{3+} substituted for Al^{3+} at the two octahedral positions inside the XRD-coherent domains (Fe^{3+} in site II). The influence of Fe^{3+} ions in site I, i.e., probably at the periphery of the crystalline domains, would then be negligible.

FTIR reflectance spectrometry in the NIR domain appears to be a very simple and powerful tool for the quantitative comparison of Fe^{3+} substituted in kaolinite. The method is, however, more difficult to implement in the case of kaolinites with high contents of phyllosilicates impurities or with surface areas higher than 30 m^2/g. The use of spectral reflectance measurements in the near-infrared (NIR) wavelength domain minimizes two significant problems associated with MIR transmission measurements of clay minerals: 1) reflectance-IR measurements can usually be carried out without grinding the samples (indeed, extensive grinding associated with the preparation of extremely fine materials for dispersion in KBr pellets can affect clay minerals); and 2) The amount of sample analyzed in the reflectance-IR mode is much higher than in the transmission mode, reducing the doubts regarding the representative nature of the sample. Reflectance spectroscopy is a sensitive diagnostic tool for environmental geochemistry, as structural Fe is a witness of the growth conditions of kaolinite (Cases *et al.*, 1986; Muller and Calas, 1993).

ACKNOWLEDGMENTS

The study of sedimentary and reference kaolinites was supported by the French Ministère de la Recherche et de la Technologie, the Institut National des Sciences de l'Univers (CNRS), and by the Argiles et Minéraux–AGS company (Montguyon, Charentes, France) through Grant 89 R 0470. The study of soil kaolinites was supported by the PEGI (CNRS-INSU-ORSTOM) program. The authors are most grateful to B. Morin for technical assistance in EPR measurements.

REFERENCES

Allard, T., Malengreau, N., Muller, J. P. (1992) Approche spectroscopique de la typologie des kaolins des Charentes: *Colloque bilan VRM 4 12 1992,* Ministère de la Recherche et de la Technologie, Paris, 461–478.

Angel, B. R. and Vincent, W. E. J. (1978) Electron spin resonance studies of iron oxides associated with the surface of kaolins: *Clays & Clay Minerals* **26,** 263–272.

Barrios, J., Plançon, A., Cruz, M. J., and Tchoubar, C. (1977) Qualitative and quantitative study of stacking faults in a hydrazine treated kaolinite. Relationships with the infrared spectra: *Clays & Clay Minerals* **25,** 422–429.

Bonnin, D., Muller, S., and Calas, G. (1982) Le fer dans les kaolins. Etude par spectométries RPE, Mössbauer, EXAFS: *Bull. Minéral.* **105,** 467–475.

Braun, J. J., Pagel, M., Muller, J. P., Bilong, P., Michard, A., and Guillet, B. (1990) Cerium anomalies in lateritic profiles: *Geochim. Cosmochim. Acta* **54,** 781–795.

Brindley, W. G., Kao, C. C., Harrison, J. L., Lipsicas, M., and Raythatha, R. (1986) Relation between structural disorder and other characteristics of kaolinites and dickites: *Clays & Clay Minerals* **34,** 239–249.

Calas, G. (1988) Electron paramagnetic resonance: in *Spectroscopic Methods in Mineralogy and Geology,* F. C. Hawthorne, ed., Mineralogical Society of America, Reviews in Mineralogy **18,** 513–563.

Cases, J. M., Lietard, O., Yvon, J., Delon, J. F. (1982) Etude des propriétés cristallochimiques, morphologiques et superficielles de kaolinites désordonnées: *Bull. Mineral.* **105,** 439–457.

Cases, J. M., Cunin, Ph., Grillet, Y., Poinsignon, Ch., Yvon, J. (1986) Methods of analyzing morphology of kaolinite: Relations between crystallographic and morphological properties: *Clay Miner.* **21,** 55–68.

Crowley, J. K. and Vergo, N. (1988) Near-infrared reflectance spectra of mixtures of kaolin-group minerals: Use in clay minerals studies: *Clays & Clay Minerals* **36,** 310–316.

Delineau, T., Yvon, J., Cases, J. M., Villieras, F. (1992) Variabilité des kaolins des Charentes: Recherche typologique, guides d'applications: *Colloque bilan VRM 4 12 1992,* Ministère de la Recherche et de la Technologie, Paris, 413–436.

Delvaux, B., Mestdagh, M. M., Vielvoye, L., and Herbillon, A. J. (1989) XRD, IR and ESR study of experimental alteration of Al-nontronite into mixed-layer kaolinite/smectite: *Clay Miner.* **24,** 617–630.

Dubreuilh, J., Marchadour, P., and Thiry, M. (1984) Cadre géologique et mineralogie des argiles des Charentes, France: *Clay Miner.* **19,** 29–41.

Fripiat, J. J. and van Olphen, H. (1979) *Data Handbook for Clay Materials and Other Non-Metallic Minerals:* Pergamon Press, New York, 319–333.

Gaite, J. M., Ermakoff, P., and Muller, J. P. (1993) Characterization and origin of two Fe^{3+} EPR spectra in kaolinite: *Phys. Chem. Miner.* **20,** 242–247.

Giese, R. F. (1988) Kaolin minerals. Structures and stabilities: in *Hydrous Phyllosilicates, Reviews in Mineralogy* **19,** S. W. Bailey, ed., Mineralogical Society of America, Washington, D.C., 29–66.

Hall, P. L. (1980) The application of electron spin resonance to studies of clay minerals. I. Isomorphous substitution and external surface properties: *Clay Miner.* **15,** 312–335.

Herbillon, A. J., Mestdagh, M. M., Virevoye, L., and Derouane, E. G. (1976) Iron in kaolinite with special reference from tropical soils: *Clay Miner.* **11,** 201–220.

Hunt, G. R. and Salisbury, J. W. (1970) Visible and near infrared spectra of minerals and rocks: I. Silicates minerals: *Mod. Geology* **1,** 283–300.

Hunt, G. R. (1977) Spectral signatures of particulate minerals in the visible and near infrared: *Geophysics* **42,** 501–513.

Kato, E., Kanaoha, S., and Inagahi, S. (1977) Infrared spectra of kaolin minerals in OH regions. I. On the glass slide methods for the measurement of the infrared spectra in OH region of clay minerals: *Rept. Govt. Industr. Res. Inst. Agoya.* **26,** 203–210.

Kemp, R. C. (1973) Electron spin resonance of iron (3+) in muscovite: *Phys. Stat. Sol.,* B57, K79–K81.

Jackson, N. J., Willis-Richard, J., Manning D. A. C., and Sams, M. S. (1989) Evolution of the Cornubian ore field, Southwest England. Part II. Mineral deposits and ore-forming processes: *Econ. Geol.* 84, 1101–1133.

Jones, J. P. E., Angel, B. R., Hall, P. L. (1974) Electron spin resonance studies of doped synthetic kaolinites: *Clay Miner.* **10,** 257–270.

Ledoux, R. L. and White, J. L. (1964) Infrared studies of the hydroxyl group in intercalated kaolinite complexex: *Clays and Clay Minerals, Proc. 13th Natl. Conf., Madison, Wisconsin, 1964,* W. F. Bradley and S. W. Bailey, eds., Pergamon Press, New York, 289–315.

Lietard, O. (1977) Contribution à l'étude des propriétés physicochimiques, cristallographiques et morphologiques des kaolins: *Thèse doct. es sci.* INPL Nancy, 321 pp.

Meads, R. E. and Malden, P. J. (1975) Electron spin resonance in natural kaolinites containing Fe^{3+} and other transition metal ions: *Clay Miner.* **10,** 313–345.

Mehra, O. P. and Jackson, M. L. (1960) Iron oxide removal from soil and clays by a dithionite-citrate system buffered with sodium carbonate: in *Proc. 7 th. Natl. Conf. on Clays and Clay Minerals,* A. Swineford, ed., Pergamon Press, Washington, D.C., 317–327.

Mendelovici, E., Yariv, S. H., and Villaba, R. (1979) Iron bearing kaolinite in Venezuelan laterite. I. Infrared spectroscopy study and chemical dissolution evidence: *Clay Miner.* **14,** 323–327.

Mestdagh, M. M., Vielvoye, L., and Herbillon, A. J. (1980) Iron in kaolinite. II. The relationships between kaolinite crystallinity and iron content: *Clay Miner.* **15,** 1–14.

Muller, J. P. (1988) Analyse pétrologique d'une formation latéritique meuble du Cameroun. Essai de traçage d'une différenciation supergène par les paragenèses minérales secondaires: *Thèse Doct. es-Sciences,* Université de Paris VII, ORSTOM. Pub., Paris, 188 pp.

Muller, J. P. and Bocquier, G. (1986) Dissolution of kaolinites and accumulation of iron oxides in lateritic-ferruginous nodules. Mineralogical and microstructural transformations: *Geoderma* **37,** 113–136.

Muller, J. P. and Bocquier, G. (1987) Textural and mineralogical relationships between ferruginous nodules and surrounding clayey matrices in a laterite from Cameroon: in *Proc. Intern. Clay Conf., Denver, 1985,* L. G. Schultz, H. van Olphen, and F. A. Mumpton, eds., The Clay Minerals Society, Bloomington, Indiana, 186–196.

Muller, J. P. and Calas, G. (1989) Tracing kaolinites through their defect centers; Kaolinite paragenesis in a laterite (Cameroon): *Econ. Geol.* **84,** 694–707.

Muller, J. P. and Calas, G. (1993) Genetic significance of paramagnetic centers in kaolinites: in *Keller Kaolin 90 Symp.,* M. Bundy, H. H. Murray, and C. C. Harvey, eds., The Clay Minerals Society, Boulder, Colorado, 261–289.

Muller, J. P., Ildefonse, Ph., and Calas, G. (1990) Paramagnetic defect centers in hydrothermal kaolinite from an altered tuff in the Nopal uranium deposit, Chihuahua, Mexico: *Clays & Clay Minerals* **38,** 600–608.

Murray, H. H. (1988) Kaolin minerals: Their genesis and occurrences: in *Hydrous Phyllosilicates, Reviews in Mineralogy* **19,** S. W. Bailey, ed., Mineralogical Society of America, Washington, D. C., 67–90.

Olivier, D., Védrine, J. C., and Pézerat, H. (1975) Application de la RPE à la localisation du fer^{3+} dans les smectites: *Bull. Groupe Français des Argiles* **27,** 153–165.

Petit, S. and Decarreau, A. (1990) Hydrothermal (200°C) synthesis and crystal chemistry of iron rich kaolinite: *Clay Miner.* **25,** 181–196.

Pinnavaia, T. J. (1981) Electron spin resonance studies of clay minerals: in *Advanced Techniques for Clay Minerals Analysis, Developments in Sedimentology* **34,** J. J. Fripiat, ed., Elsevier, Amsterdam, 139–161.

Plançon, A., Giese, R. F., and Snyder, R. (1988) The Hinckley index for kaolinites: *Clay Miner.* **23,** 249–260.

Simmons, E. L. (1971) An equation relating the diffuse reflectance of weakly absorbing powdered samples to the fundamental optical parameters: *Optica Acta* **18,** 59–68.

Yvon, J., Liétard, O., Cases, J. M., and Delon, J. F. (1982) Minéralogie des argiles kaoliniques des charentes: *Bull Miner.* **105,** 431–437.

(Received 9 July 1993; accepted 22 December 1993; Ms. 2400)